Biomech Model Mechanobiol (2010) 9:671–687
DOI 10.1007/s10237-010-0204-z

ORIGINAL PAPER

# A model for arterial adaptation combining microstructural collagen remodeling and 3D tissue growth

**I. M. Machyshyn · P. H. M. Bovendeerd · A. A. F. van de Ven · P. M. J. Rongen · F. N. van de Vosse**

Received: 2 April 2009 / Accepted: 25 February 2010 / Published online: 19 March 2010


**Abstract** Long-term adaptation of soft tissues is realized through growth and remodeling (G&R). Mathematical models are powerful tools in testing hypotheses on G&R and supporting the design and interpretation of experiments. Most theoretical G&R studies concentrate on description of either growth or remodeling. Our model combines concepts of remodeling of collagen recruitment stretch and orientation suggested by other authors with a novel model of general 3D growth. We translate a growth-induced volume change into a change in shape due to the interaction of the growing tissue with its environment. Our G&R model is implemented in a finite element package in 3D, but applied to two rotationally symmetric cases, i.e., the adaptation towards the homeostatic state of the human aorta and the development of a fusiform aneurysm. Starting from a guessed non-homeostatic state, the model is able to reproduce a homeostatic state of an artery with realistic parameters. We investigate the sensitivity of this state to settings of initial parameters. In addition, we simulate G&R of a fusiform aneurysm, initiated by a localized degradation of the matrix of the healthy artery. The aneurysm stabilizes in size soon after the degradation stops.

**Keywords** Artery · Aneurysm · Remodeling · Growth · Collagen

I. M. Machyshyn · P. H. M. Bovendeerd (✉) · F. N. van de Vosse
Biomedical Engineering, Eindhoven University of Technology, Eindhoven, The Netherlands
e-mail: p.h.m.bovendeerd@tue.nl

A. A. F. van de Ven
Mathematics and Computing Science, Eindhoven University of Technology, Eindhoven, The Netherlands

P. M. J. Rongen
Philips Medical Systems, Best, The Netherlands

## 1 Introduction

Arteries adapt to sustained changes in their environment, e.g., changes in blood pressure or shear stress, both by growth and remodeling (G&R). Following Humphrey and Rajagopal (2002) *growth* is defined as "an increase in mass that is achieved locally via an increase in the number of cells and/or via a synthesis of extracellular matrix that exceeds removal", and *remodeling* as "a change in structure that is achieved by reorganizing existing constituents or by synthesizing new constituents that have a different organization". Remodeling may involve the composition of the tissue, i.e., the relative amounts of the most important mechanically contributing components, such as elastin, collagen and smooth muscle cells. It may also involve the orientation of the collagen fibers. While it is generally recognized that mechanical load is a stimulus for G&R, it is still unknown what aspect of mechanical load is related to what aspect of G&R. A mathematical model can be used to elucidate the stimulus–effect relation, since it can be used to test hypotheses on G&R. In a later stage, it could be used to predict arterial G&R in disease and upon surgical intervention, and help in designing protocols in tissue engineering.

Earliest mathematical models of G&R focussed on growth. Inspired by Skalak et al. (1982), Rodriguez et al. (1994) formulated a growth model in which a stimulus for growth was translated into a growth tensor, describing the growth of virtual infinitesimal, isolated tissue elements. To join these virtual elements into a continuous intact tissue, an additional elastic deformation was introduced, which was considered to be the origin of the residual stresses and strains, observed in arteries. In a number of subsequent studies (e.g., Taber and Eggers 1996; Taber 1998; Taber and Humphrey 2001; Kuhl et al. 2007), this idea was applied to the stress-driven growth of an artery. An alternative growth model was

introduced by Rachev et al. (1996), where growth is described by evolving zero-stress states of the artery, driven by the tissue stress as well. Klisch et al. (2001) presented a theoretical framework for incremental growth of compressible elastic tissues. In all of these studies, tissue growth is governed by a growth tensor defined for specific geometries, whereas no general definition of the growth tensor for arbitrary geometries is provided. In addition, these studies are phenomenological, in a sense that they do not consider changes in the microstructure of the tissue, such as changes in composition or collagen fiber orientations.

Later, other models have focussed on tissue remodeling. In the model by Watton et al. (2004), the tissue consists of a mixture of elastin and collagen. At each point in the tissue, the collagen is characterized by two fiber directions and two normalized collagen fiber densities. In addition, the zero-stress state for collagen is allowed to differ from that of elastin by the introduction of a collagen recruitment stretch. Tissue adaptation is modeled by the evolution of the normalized collagen fiber densities and the recruitment stretches, driven by collagen stretch. A restriction of the model is that fiber directions and tissue volume remain constant. Recently, this model was adopted in Watton and Hill (2009) for modeling development of abdominal aortic aneurysms, and in Watton et al. (2009) for modeling development of cerebral aneurysms. In the model by Driessen et al. (2004), the tissue consists of a mixture of elastin and collagen as well. Here, the collagen is characterized by its volume fraction and four fiber directions, but the zero-stress states for elastin and collagen are assumed identical. Tissue adaptation is modeled by the evolution of the collagen volume fraction and the fiber directions, driven by principal tissue stresses or strains. While volume fraction may change, total tissue volume remains constant. In Driessen et al. (2005, 2008), the model was extended by incorporating a spatial distribution of collagen fiber orientations. The model of Hariton et al. (2007) is similar to that of Driessen et al. (2004). A limitation of these models is that tissue growth is only formally taken into account by adjusting coefficients of constitutive relations rather than realizing 3D volume change associated with the change of mass.

A more microstructural approach to model G&R was suggested by Humphrey and Rajagopal (2002), who considered a tissue to be a mixture of several constituents. As a constituent ages, it is gradually degraded. Simultaneously, new constituents are synthesized, with a configuration determined by the actual tissue load. At each moment in time, the tissue consists of families (or generations) of constituents, deposited at different moments of time in the past, each of which may have its own zero-stress state. Remodeling naturally follows from differences in properties between new and degraded generations. This idea was applied to describe G&R of the arterial wall by (among others) Gleason et al. (2004), Baek et al. (2005, 2006), and Kroon and Holzapfel (2007). These models are restricted to membrane structures, in which volume growth is incorporated through a change in membrane thickness. Alford et al. (2008) extended these models by combining the theory for microstructural matrix remodeling of Humphrey and Rajagopal (2002) and the theory for volumetric growth of Rodriguez et al. (1994) with smooth muscle contraction included by the method of Taber (2000). Special attention there is paid to the concept of residual stresses, in particular to opening angles occurring when unloaded arteries spring open if cut transmurally. The geometry of the model is restricted to a thick-walled tube under axisymmetrical loading. Recently, Valentin et al. (2009) presented a model using the extended mixture model by Humphrey and Rajagopal (2002) combined with smooth muscle contraction. The model accounts for the regulatory effect of altered wall shear stress on extracellular matrix turnover. The model is formulated in a 2D mechanics approach and applied to study arterial adaptations to altered flow and pressure.

The aim of this study is to develop a generic microstructurally based model of 3D arterial G&R applicable to arbitrary tissue configurations. Towards this end, we present a model combining microstructural matrix remodeling (Humphrey and Rajagopal 2002) and microstructural description of collagen architecture (Driessen et al. 2008) with a new general 3D growth model. In our growth model, a growth stimulus is translated into a scalar, representing an unconstrained volume change of a local tissue element. The latter is converted into an actual change of volume and shape of the tissue element as a result of mechanical interaction of the element with neighboring elements, thus keeping the deformation of the tissue as a whole compatible. We focus on the integration of the two existing models with the new 3D growth model and use a simple model of tissue composition (collagen and matrix) and stimulus for G&R (collagen stretch). The model is illustrated by simulation of adaptation towards a homeostatic state of the aorta, and development of a fusiform aneurysm.

## 2 Methods

### 2.1 Configurations

Arterial G&R is modeled as a discrete sequence of continuously changing tissue configurations. To explain the model, we introduce three configurations: the unloaded configuration $\boldsymbol{\mathcal{C}}_0(t)$, the loaded configuration $\boldsymbol{\mathcal{C}}(t)$ and the grown configuration $\boldsymbol{\mathcal{C}}_0(t+\Delta t)$. Configuration $\boldsymbol{\mathcal{C}}_0(t)$ corresponds to the tissue free of both external and internal stress. Configuration $\boldsymbol{\mathcal{C}}(t)$ corresponds to the externally loaded tissue, and is related to $\boldsymbol{\mathcal{C}}_0(t)$ through an incompressible loading deformation gradient tensor $\boldsymbol{\mathcal{F}}_l(t)$, describing the instantaneous response of the tissue to the loading. Configuration $\boldsymbol{\mathcal{C}}_0(t+\Delta t)$

corresponds to the grown tissue, and is related to $\mathcal{C}_0(t)$ through a growth deformation gradient tensor $\mathcal{F}_g(t)$, describing volume and shape change without any external loading. The latter configuration serves as the new unloaded configuration for time step $t + \Delta t$.

### 2.2 The unloaded configuration

The arterial wall consists of many components, among which are elastin, collagen and smooth muscle cells embedded in ground substance. Together, the collagen fibers form the collagen component. We group all non-collagenous material into one component, referred to as the matrix. Like many biological tissues, arteries undergo constant renewal or remodeling. Rates of the turnover of different components of the artery vary a lot. For instance, the half-life of collagen is 3–90 days in various soft tissues, while that of elastin is in the order of years (Humphrey 1999). In our model, we assume that the rate of turnover of the matrix is negligible if compared to the rate of turnover of collagen. In view of this relatively fast turnover of collagen, we use the concept of a collagen generation, defined as the amount of collagen generated in a certain time interval $\Delta t$. We distinguish between $N$ collagen generations; all the generations created longer than the time span $N\Delta t$ ago are assumed to be fully degraded at the actual moment in time. For each generation, we follow the idea suggested by Driessen et al. (2008) that collagen fibers are distributed along $K$ fiber directions. Within a generation $i$, $i \in \overline{1, N}$, with a collagen volume fraction $n_{c,i}$, we define the volume fraction $n_{c,ij}$ of the collagen fibers oriented in the range of directions $(\gamma_j - \Delta\gamma, \gamma_j)$ as

$$\begin{aligned} n_{c,ij}(t) &= n_{c,i}(t)\ \hat{D}_i(\gamma_j)\ \Delta\gamma, \\ \hat{D}_i(\gamma_j) &= \frac{D_i(\gamma_j)}{\sum_{k=1}^{K} D_i(\gamma_k)\Delta\gamma}, \end{aligned} \tag{1}$$

where $\hat{D}_i(\gamma_j)$ is a normalized discrete distribution function (for the definition of the distribution function $D_i(\gamma_j)$ see (22) further on), $\gamma_j = -\pi/2 + \pi j/K$, $j = \overline{1, K}$, and $\Delta\gamma = \pi/K$. Note here that $n_{c,i}(t)$ is the volume fraction at the current time $t$ of the collagen created at $t - (i-1)\Delta t$, taken with respect to the current volume at time $t$.

Definition (1) ensures that the volume fractions $n_{c,ij}$ of all fibers within a generation $i$ add up to the volume fraction of this generation $n_{c,i}$, or

$$n_{c,i} = \sum_{j=1}^{K} n_{c,ij}. \tag{2}$$

In addition, the volume fractions of all components add up to one:

$$n_m + \sum_{i=1}^{N} n_{c,i} \equiv n_m + n_{c,\mathrm{tot}} = 1, \tag{3}$$

where $n_m$ represents the volume fraction of the matrix and $n_{c,\mathrm{tot}}$ the total volume fraction of collagen. We complete the description of the current unloaded state by noting that fibers may be undulated in this state. The degree of undulation of a fiber in generation $i$ along direction $\gamma_j$ is quantified through the recruitment stretch $\lambda_{\mathrm{rec},ij}$. The recruitment stretch represents the stretch of the matrix along direction $\gamma_j$ at which the collagen fiber becomes straight, but not yet stretched.

### 2.3 The loaded configuration

To describe the transition of the unloaded configuration into the loaded configuration, we need to assign constitutive properties to the tissue. According to the constrained mixture model of Humphrey and Rajagopal (2002), we assume no relative motion between the two components of the tissue (matrix and collagen). Moreover, we take the two components intrinsically incompressible. Since we allow no volumetric growth during the instantaneous transition from $\mathcal{C}_0(t)$ to $\mathcal{C}(t)$, described by $\mathcal{F}_l$, the whole tissue is incompressible during this phase. Then the Cauchy stress can be defined as

$$\mathcal{T} = -p\mathcal{I} + \mathcal{T}_m + \mathcal{T}_c, \tag{4}$$

with $p$ the pressure term inherent to the incompressibility of the tissue, $\mathcal{I}$ the second-order unity tensor, and $\mathcal{T}_m$ and $\mathcal{T}_c$ the stress tensors of the matrix and collagen, respectively.

The matrix is described by a Neo-Hookean material law with the following constitutive relation in the actual loaded configuration $\mathcal{C}(t)$:

$$\mathcal{T}_m = n_m\, c_m\, (\mathcal{B}_l - \mathcal{I}), \tag{5}$$

where $c_m$ is the shear modulus of the matrix, and $\mathcal{B}_l = \mathcal{F}_l \mathcal{F}_l^T$ is the left Cauchy-Green deformation tensor. The constitutive law for collagen was based on Driessen et al. (2005), but extended to account for multiple fiber generations

$$\begin{aligned} \mathcal{T}_c = {} & n_{c,\mathrm{tot}}\, c_m\, (\mathcal{B}_l - \mathcal{I}) \\ & + \sum_{i=1}^{N}\sum_{j=1}^{K} n_{c,ij} \left[ \tau_f(\lambda_{c,ij}) - \frac{1}{n_m}\, \mathbf{e}_{c,ij} \cdot \mathcal{T}_m\, e_{c,ij} \right] \\ & \times \mathbf{e}_{c,ij} \otimes \mathbf{e}_{c,ij}, \end{aligned} \tag{6}$$

where $\mathbf{e}_{c,ij}$ is the actual direction of collagen fiber $j$ of generation $i$ in loaded configuration $\mathcal{C}(t)$. According to (6), the stress–strain relation for collagen in the fiber direction $\mathbf{e}_{c,ij}$ yields a collagen stress equal to $n_{c,ij}\ \tau_f(\lambda_{c,ij})$, whereas in the cross-fiber direction the collagen behaves in the same way as the matrix. Along their directions, the fibers are assumed to exert zero compressive resistance, and the tensile constitutive

relation for the fibers is taken from (Holzapfel et al. 2000)

$$\tau_f(\lambda_{c,ij}) = 2k_1\,\lambda_{c,ij}^2\,\left(\lambda_{c,ij}^2-1\right)\exp\left[k_2\left(\lambda_{c,ij}^2-1\right)^2\right],\quad \lambda_{c,ij}>1, \tag{7}$$

with $k_1$ and $k_2$ material constants, and $\lambda_{c,ij}$ the stretch of collagen fibers, defined as the tissue stretch at $t$ in the direction $\mathbf{e}^0_{c,ij}$ divided by the recruitment stretch:

$$\lambda_{c,ij}(t) = \frac{\sqrt{\mathbf{e}^0_{c,ij}\cdot\mathcal{C}_l(t)\mathbf{e}^0_{c,ij}}}{\lambda_{\mathrm{rec},ij}}, \tag{8}$$

with $\mathcal{C}_l = \mathcal{F}_l^T\mathcal{F}_l$ the right Cauchy-Green strain tensor, and $\mathbf{e}^0_{c,ij}$ the fiber orientation in $\boldsymbol{\mathcal{C}}_0(t)$ of the same material collagen fiber having direction $\mathbf{e}_{c,ij}$ in $\boldsymbol{\mathcal{C}}(t)$. The recruitment stretch $\lambda_{\mathrm{rec},ij}$ is defined as the stretch of the matrix in the direction $\mathbf{e}_{c,ij}$ at the time of creation of generation $i$, divided by the homeostatic collagen stretch $\lambda_c^{\mathrm{hom}}$, as expressed later in (25). The homeostatic collagen stretch is the pre-stretch of new collagen generations at the moment of their deposition (Humphrey and Rajagopal 2002).

The immediate response of the tissue to an external load is governed by the equation of conservation of momentum, which after neglecting inertia and body forces reduces to the equation of mechanical equilibrium

$$\operatorname{div}\mathcal{T} = \mathbf{0}, \tag{9}$$

complemented by appropriate boundary conditions. The incompressibility of the tissue imposes an additional restriction on the deformation

$$\det(\mathcal{F}_l) = 1. \tag{10}$$

Knowing the loaded configuration, from the stretch $\lambda_{c,ij}$ of all collagen fibers, we can determine the average collagen stretch $\bar{\lambda}_c(t)$ as

$$\bar{\lambda}_c(t) = \frac{\sum_{i=1}^{N} n_{c,i}(t)\,\sum_{j=1}^{K}\lambda_{c,ij}(t)}{K\,\sum_{i=1}^{N} n_{c,i}(t)}. \tag{11}$$

This average collagen stretch plays an important role in the step towards the grown configuration.

## 2.4 The grown configuration

### *2.4.1 Evolution of tissue shape and volume*

As described before, collagen is in a state of constant turnover: existing generations of collagen decay and are replaced by new generations of collagen. We introduce the unconstrained rate of collagen production $\dot{m}_c^{\mathrm{unc}}(t)$ by the following relation:

$$\begin{aligned}\dot{m}_c^{\mathrm{unc}}(t) &= \dot{m}_c^{\mathrm{hom}}(t) + K_g\left(\bar{\lambda}_c(t)-\lambda_c^{\mathrm{hom}}\right)\\ &\equiv \dot{m}_c^{\mathrm{hom}}(t) + \dot{m}_c^{\mathrm{unc,add}},\end{aligned} \tag{12}$$

where 'unconstrained' means not restricted by the presence of surrounding tissue. Here, $\dot{m}_c^{\mathrm{hom}}(t)$ represents the rate of homeostatic production of collagen mass per unit of time and per unit of tissue volume, i.e., the rate of production of collagen that exactly compensates for the decay of old collagen generations, when the tissue is at homeostasis. The second term represents the rate of additional collagen production $\dot{m}_c^{\mathrm{unc,add}}$ when the tissue is not at homeostasis. In this term, $K_g$ is the rate constant of the mass change and $\bar{\lambda}_c(t)$ the average collagen stretch defined in (11). The unconstrained additional collagen production is assumed to be proportional to the deviation of the average collagen stretch from the homeostatic value, because at homeostasis, the average collagen stretch equals the homeostatic stretch $\lambda_c^{\mathrm{hom}}$.

Development of aneurysms is accompanied by degradation of elastin (see, e.g., He and Roach 1994; Carmo et al. 2002; Frösen et al. 2004). We model this as a degradation of the matrix. We assume that the volume fraction of the matrix with respect to the unloaded reference configuration $\boldsymbol{\mathcal{C}}_0(0)$ is given by a prescribed function $n_m^{\mathrm{ref}}(t)$. The volume fraction in the current state $\boldsymbol{\mathcal{C}}(t)$ is then

$$n_m(t) = \frac{n_m^{\mathrm{ref}}(t)}{J_g^{\mathrm{tot}}(t-\Delta t)} \tag{13}$$

where $J_g^{\mathrm{tot}}(t-\Delta t)$ is the total volume change of a reference elementary volume from $t=0$ to the current time $t$. This implies that, for $t>0$,

$$J_g^{\mathrm{tot}}(t-\Delta t) = J_g(0)\cdot J_g(\Delta t)\cdots J_g(t-\Delta t), \tag{14}$$

where $J_g(t)$ is the relative volume change from $t$ to $t+\Delta t$ as defined in (17), further on. Note that by definition, $J_g^{\mathrm{tot}}(-\Delta t)=1$. In analogy with the rate of collagen production, we introduce the rate of change of matrix mass per unit current volume $\dot{m}_m(t)$ as:

$$\dot{m}_m(t) = \frac{\rho_m}{J_g^{\mathrm{tot}}(t-\Delta t)}\frac{\mathrm{d}}{\mathrm{d}t}n_m^{\mathrm{ref}}(t) \tag{15}$$

where $\rho_m$ represents matrix mass density. To describe matrix degradation, $n_m^{\mathrm{ref}}(t)$ would be chosen to decrease with time, and consequently $\dot{m}_m(t)$ would be negative.

Within the concept of collagen generations, a new collagen generation is deposited over a time interval $\Delta t$, yielding per unit of current tissue volume an unconstrained extra collagen mass equal to $\dot{m}_c^{\mathrm{unc,add}}\Delta t$. The change in mass due to matrix degradation equals $\dot{m}_m\Delta t$. Due to this change of mass, the volume of the tissue as a whole would change by a fraction $J_g^{\mathrm{unc}}$, equal to

$$J_g^{\text{unc}}(t) = 1 + \frac{\dot{m}_c^{\text{unc,add}}\,\Delta t}{\rho_c} + \frac{\dot{m}_m(t)\Delta t}{\rho_m}, \tag{16}$$

where $\rho_c$ represents the mass density of collagen. The unconstrained volume change $J_g^{\text{unc}}$ represents the growth of an infinitesimally small *isolated* tissue element. We assume that actual *in situ* volumetric growth of the tissue element $J_g$ will deviate from unconstrained growth due to mechanical interaction with the neighboring tissue. The actual volumetric growth $J_g$ is determined as

$$J_g(t) = \det(\mathcal{F}_g(t)). \tag{17}$$

where $\mathcal{F}_g$ represents the actual growth deformation tensor. This tensor is determined from the mechanical interaction of adjacent tissue elements during growth. The grown configuration is governed by the equation of mechanical equilibrium

$$\operatorname{div} \mathcal{T}_g = \mathbf{0}, \tag{18}$$

where the growth stress $\mathcal{T}_g$ represents the internal stresses induced by growth. While we consider the tissue to be incompressible at the time scale of mechanical loading, as expressed in (4) and (10), we consider it to be compressible at the time scale of growth, to allow for volumetric growth. Therefore, we use a compressible form of (4) and (5) and arrive at a compressible Neo-Hookean constitutive relation

$$\mathcal{T}_g = \kappa \left(J_g - J_g^{\text{unc}}\right)\mathcal{I} + \frac{n_m\, c_m}{J_g}\left(\mathcal{B}_g - J_g^{2/3}\mathcal{I}\right), \tag{19}$$

with bulk modulus $\kappa$, and $\mathcal{B}_g = \mathcal{F}_g\mathcal{F}_g^T$. Equation (19) shows how the unconstrained volume change $J_g^{\text{unc}}$ is considered as a local internal load on the tissue. The extent to which the true volume change $J_g$ deviates from the unconstrained volume change $J_g^{\text{unc}}$ depends on the ratio between $\kappa$ and $c_m$. Though in reality growth takes place in the loaded configuration, we simulate growth in the externally unloaded state. Since in this state collagen fibers are undulated and carry no stress, we neglect the contribution of collagen in (19).

The position $\mathbf{x}_0(t)$ of a tissue element in the unloaded configuration $\mathcal{C}_0(t)$ is updated to $\mathbf{x}_0(t+\Delta t)$ in the unloaded configuration $\mathcal{C}_0(t+\Delta t)$ according to:

$$\mathbf{x}_0(t+\Delta t) = \mathbf{x}_0(t) + \mathbf{u}_g(t), \tag{20}$$

where $\mathbf{u}_g(t)$ is the displacement due to growth from $t$ to $t+\Delta t$. Finally, we assume the growth-induced stress $\mathcal{T}_g$ to disappear in time due to remodeling of the matrix. Thus, the new externally unloaded configuration $\mathcal{C}_0(t+\Delta t)$ is assumed to be internally free of stress.

### 2.4.2 Properties of the new collagen generation

The volume fraction of the new collagen generation can be computed straightforwardly as (note that $i = 1$ refers to the current time $t$)

$$n_{c,1}(t+\Delta t) = \frac{\dot{m}_c(t)\,\Delta t}{\rho_c\, J_g(t)} = \frac{\Delta t}{J_g(t)}\left(\frac{\dot{m}_c^{\text{hom}}(t)}{\rho_c} - \frac{\dot{m}_m(t)}{\rho_m}\right) + \frac{J_g(t)-1}{J_g(t)}, \tag{21}$$

where $\dot{m}_c(t)$ is the rate of real production of collagen. This real rate of collagen production is determined from (12) using (16). Before determining $\dot{m}_c(t)$, the superscript 'unc' should be skipped in both aforementioned relations because the true volume change $J_g(t)$ defined by (17) is used in (16) instead of the unconstrained volume change $J_g^{\text{unc}}(t)$. To evaluate the right-hand side of (21), we use relations (15), (16), and (31) further on.

Direction and recruitment length of the fibers in the new generation are assumed to depend on the loading state of the tissue. Fibers are created in a plane, spanned by the principal stretch directions $\mathbf{v}_1$ and $\mathbf{v}_2$ of the left Cauchy-Green deformation tensor $\mathcal{B}_l(t)$, with associated largest and second largest tissue stretch $\lambda_1$ and $\lambda_2$. Fiber orientation is described by the distribution function $D_1(\gamma_j)$ in (1). The specific shape of this function is taken from Driessen et al. (2008):

$$D_1(\gamma_j) = \mathrm{e}^{-\frac{1}{\sigma}}\left\{\exp\left(\frac{\cos[2(\gamma_j-\mu)]}{\sigma}\right) + \exp\left(\frac{\cos[2(\gamma_j+\mu)]}{\sigma}\right)\right\}, \tag{22}$$

with $\gamma_j$ the angle between the fiber direction and the principal stretch direction $\mathbf{v}_1$ ($\gamma_j = -\pi/2 + \pi j/K$, $j = \overline{1,K}$), $\pm\mu$ the mean fiber directions, and $\sigma$ the width of the distribution. The distribution function (22) is the sum of two subdistribution functions with the same width $\sigma$, and mean fiber angles $\mu$ and $-\mu$. A representative distribution function $D_1(\gamma)$ together with the subdistribution functions is shown in Fig. 1. The parameters of the distribution, following Driessen et al. (2008), are given by

$$\sigma = \begin{cases} \dfrac{k}{g_1/g_2 - 1}, & g_1 \geq g_2, \\ \dfrac{k}{g_2/g_1 - 1}, & g_1 < g_2, \end{cases} \qquad \mu = \arctan\left(\frac{g_2}{g_1}\right), \tag{23}$$

where $k$ is a scaling factor of the width of the distribution, and $g_1$ and $g_2$ are the stimulus functions along the first and the second principal stretch directions. As in Driessen et al. (2008), the functions $g_1$ and $g_2$ are chosen as

$$g_1 = \lambda_1 - 1, \quad \lambda_1 > 1, \qquad g_2 = \begin{cases} \lambda_2 - 1, & \lambda_2 \geq 1, \\ 0, & \lambda_2 < 1, \end{cases} \tag{24}$$

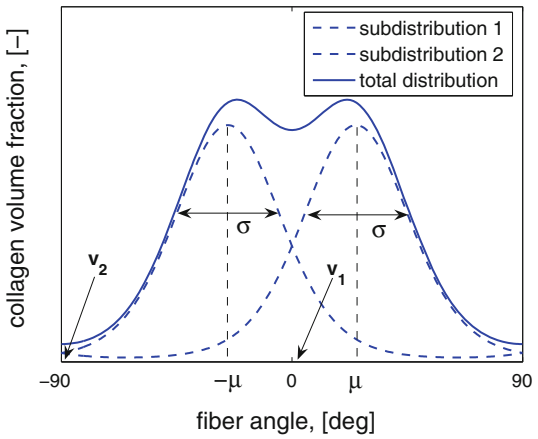


**Fig. 1** The distribution of collagen fibers in the newly deposited generation in the loaded configuration (the *solid line*). Since the mean fiber angles ($\mu$ and $-\mu$) of the subdistributions (the *dash lines*) are symmetrical with respect to the first principal stretch direction $\mathbf{v}_1$, the total distribution is symmetrical with respect to $\mathbf{v}_1$ as well. Note that the locations of the peaks of the total distribution differ from $\mu$ and $-\mu$

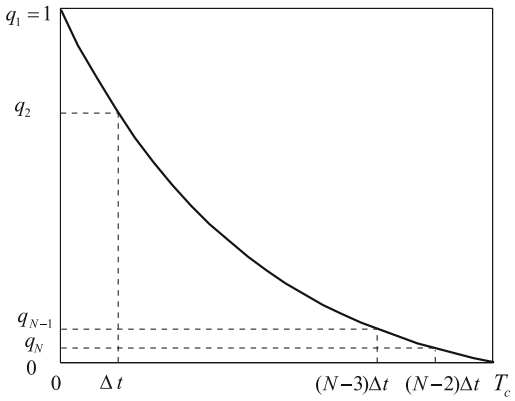


**Fig. 2** Representative survival function of collagen; $T_c = (N-1)\Delta t$

The larger the difference in principal stretches, the more the fibers align with the principal stretch direction related to the largest principal stretch.

In each direction $j$, collagen is deposited at the homeostatic stretch $\lambda_c^{\text{hom}}$, which in combination with the tissue stretch along that direction defines the recruitment stretch $\lambda_{\text{rec},1j}$ as

$$\lambda_{\text{rec},1j} = \frac{1}{\lambda_c^{\text{hom}}} \sqrt{\mathbf{e}^0_{c,1j} \cdot \mathcal{C}_l \mathbf{e}^0_{c,1j}}. \tag{25}$$

### 2.4.3 Updating properties of old collagen generations

In the grown configuration, the properties of the old collagen generations have changed. To evaluate these changes, we consider collagen of generation $i$ in an elementary tissue volume element at time $t$. The mass $\Delta M_{c,i}(t)$ of this amount of collagen is related to the mass $\Delta M^{(0)}_{c,i}(t)$ at the moment at which it was created by the following multiplicative decomposition:

$$\begin{aligned} \Delta M_{c,i}(t) &= \Delta M_c\left(t-(i-1)\Delta t\right) q_c\left((i-1)\Delta t\right) \\ &\equiv \Delta M^{(0)}_{c,i}(t)\, q_{c,i}, \quad t-(i-1)\Delta t > 0, \end{aligned} \tag{26}$$

with $i = 1$ denoting the generation deposited at the current time $t$, $i = N$ denoting the 'oldest' generation, and $q_{c,i}$ the values of a monotone decreasing survival function of collagen $q_c(t)$ at $t-(i-1)\Delta t$, i.e.,

$$q_{c,i} = q_c((i-1)\Delta t), \quad i = \overline{1, N}. \tag{27}$$

The survival function is equal to 1 for $i = 1$ ($q_{c,1} = 1$) and zero for $i = N+1$ ($q_{c,N+1} = 0$), since the oldest generation $N$ disappears completely at the next time interval. We use for $q_c(t)$ the exponential function (see Fig. 2)

$$q_c(t) = \begin{cases} e^{-nt/T_c}, & t \in [0, T_c], \\ 0, & t > T_c. \end{cases} \tag{28}$$

with $T_c$ the characteristic time of collagen degradation, and $n$ a parameter of the survival function set to $n = 3$.

At each consecutive time step, every generation becomes 'older', meaning that the generation number is increased by one, so

$$\Delta M^{(0)}_{c,i}(t+\Delta t) = \Delta M^{(0)}_{c,(i-1)}(t), \quad i = \overline{2, N}. \tag{29}$$

This relation follows trivially from the deposition of $\Delta M^{(0)}_{c,i}$ according to (26). Taking into account this shift of generations, the intrinsic degradation, and the change of the local volume of the tissue by $J_g$, the volume fractions of the generations 2 to $N$ are obtained:

$$n_{c,i}(t+\Delta t) = \frac{q_{c,i}}{q_{c,(i-1)}} \frac{n_{c,(i-1)}(t)}{J_g(t)}, \quad i = \overline{2, N}. \tag{30}$$

In the homeostatic state, at subsequent moments in time, the volume fractions of collagen generations of the same age will be identical. In addition, $J_g(t) = 1$ and $\dot{m}_c(t) = \dot{m}_c^{\text{hom}}(t)$ in this state. From these observations, using (30) and (21), we can determine the homeostatic mass production:

$$\dot{m}_c^{\text{hom}}(t) = \frac{\rho_c}{\Delta t} \sum_{i=1}^{N} n_{c,i}(t) \left(1 - \frac{q_{c,(i+1)}}{q_{c,i}}\right). \tag{31}$$

Being defined in the unloaded configuration $\mathcal{C}_0(t)$, the distribution $D_i(\gamma_j)$ for all generations ($i = \overline{1, N}$) is converted to the grown configuration using the growth deformation gradient $\mathcal{F}_g(t)$. In addition, the recruitment of a fiber decreases as the tissue grows in the direction of this fiber. We account for it by updating the recruitment stretch $\lambda_{\text{rec},ij}$ by means of $\mathcal{F}_g(t)$, as the unloaded configuration $\mathcal{C}_0(t)$ grows into $\mathcal{C}_0(t+\Delta t)$.

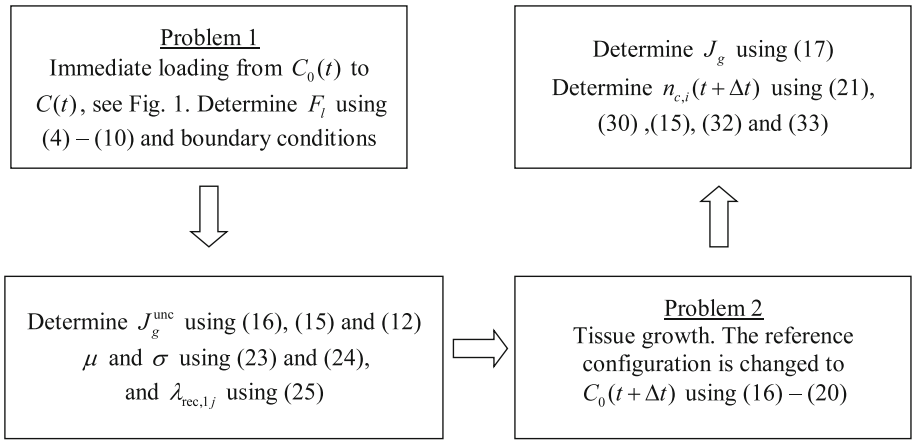


**Fig. 3** Scheme of the numerical computations

### 2.5 Implementation

The model is implemented in the finite element package Sepran (Segal 2007). The scheme of computations is presented in Fig. 3. Since different constitutive relations are used for immediate loading [(4)–(7)], and for growth [(19)], two different problem definitions for numerical calculations are used. *Problem 1* defines loading from the known unloaded configuration of the tissue $\mathcal{C}_0(t)$ to the unknown loaded configuration $\mathcal{C}(t)$, allowing to determine the deformation gradient $\mathcal{F}_l$. On calculating the average collagen stretch $\bar{\lambda}_c$, the rate of the unconstrained collagen production $\dot{m}_c^{\text{unc,add}}$ and the unconstrained volume change $J_g^{\text{unc}}$ are calculated. Using $\mathcal{F}_l$, the principal stretches and stretch directions are computed from which subsequently both parameters ($\mu$ and $\sigma$) in the distribution function $D_1$ and the recruitment stretch $\lambda_{\text{rec},1}$ of new collagen generation are determined. The unconstrained volume change is then used as an input for *Problem 2*, which defines the growth from $\mathcal{C}_0(t)$ to $\mathcal{C}_0(t+\Delta t)$. On computing the new unloaded configuration $\mathcal{C}_0(t+\Delta t)$, the real volume change and after that the volume fractions of collagen are determined.

For both problems, three-dimensional 27-node hexahedral isoparametric elements are used. For *Problem 1*, a mixed formulation with triquadratic interpolation of the displacement field and a trilinear continuous interpolation of pressure field (Taylor–Hood element), and for *Problem 2* a triquadratic interpolation of displacements is used. Being nonlinear, both problems are solved with the help of a Newton–Raphson iteration process. Material behavior is implemented through user-defined subroutines.

## 3 Application to a healthy artery and a fusiform aneurysm

To test our model, we applied it to an artery resembling the human aorta. We consider adaptation of the artery starting from an initial guessed state, and show that the homeostatic state can be reached and is physiologically acceptable. This homeostatic state is a starting state for the development of an aneurysm. We show that the aneurysm grows with time, taking a fusiform shape, and stabilizes (stops growing) when its maximum radial dimension reaches approximately twice the diameter of the healthy artery. Table 1 lists target parameters of the healthy artery. The inner radius and the ratio between the wall thickness and the radius of the artery are taken from Watton and Hill (2009). The average collagen fraction of the aorta of 0.41 was based on observations that the average collagen fraction in the media is 0.31 (Feldman and Glagov 1971) and about twice as low as in the adventitia (Fung 1993, Ch. 8), and that the media of the aorta is twice as thick as the adventitia (Watton and Hill 2009).

**Table 1** Parameters of the healthy (index (H)) artery based on literature data

| Parameter | Value | Unit | Description |
|---|---|---|---|
| $R_i^{(H)}$ | 6.6 | mm | Inner radius of an unloaded artery |
| $H^{(H)}/R_i^{(H)}$ | 0.3 | – | Ratio of the wall thickness to the inner radius of an unloaded artery |
| $n_{c,\text{tot}}^{(H)}$ | 0.41 | – | Average volume fraction of collagen |

The parameters of the model in the initial guessed state $\mathcal{C}_0$ are given in Table 2. The inner radius of the unloaded artery $R_i^{(0)}$ equals that of the healthy artery, whereas the initial ratio of the wall thickness to the inner radius $H^{(0)}/R_i^{(0)}$ is chosen lower than that of the healthy artery (compare with Table 1) to create a stimulus for G&R. The initial volume fraction of collagen $n_{c,\text{tot}}^{(0)}$ is taken lower as compared to the healthy value to create an additional stimulus for G&R , while the transmural gradient was chosen to approximate the gradient in the healthy state. The initial distribution of collagen fiber orientations is chosen uniform ($\sigma^{(0)} = \infty$, and $\mu^{(0)} = 0$). Finally, the initial recruitment stretch was tentatively set to $\lambda_{\text{rec}}^{(0)} = 1.0$.

**Table 2** Initial (index (0)) parameters of the model

| Parameter | Value | Unit | Description |
|---|---|---|---|
| $R_i^{(0)}$ | 6.6 | mm | Inner radius of an unloaded artery |
| $H^{(0)}/R_i^{(0)}$ | 0.23 | – | Ratio of the wall thickness to the inner radius of an unloaded artery |
| $n_{c,\mathrm{tot}}^{(0)}$ | 0.05, 0.3 | – | Volume fractions of collagen at the inner and at the outer surface, respectively; the distribution in the radial direction is linear |
| $\sigma^{(0)}$ | $\infty$ | – | Width of the fiber distributions |
| $\mu^{(0)}$ | 0 | deg | Mean fiber angle of collagen fiber distributions |
| $\lambda_{\mathrm{rec}}^{(0)}$ | 1.0 | – | Recruitment stretch |

**Table 3** Constitutive and loading parameters

| Parameter | Value | Unit | Description |
|---|---|---|---|
| Healthy artery and aneurysm | | | |
| $c_m$ | 100 | kPa | Shear modulus of the matrix |
| $k_1$ | 70 | kPa | Stiffness parameter of collagen fiber |
| $k_2$ | 10 | – | Material parameter of collagen |
| $\lambda_c^{\mathrm{hom}}$ | 1.1 | – | Homeostatic stretch |
| $\kappa/c_m$ | 100 | – | Bulk modulus over the shear modulus in growth relation (see (19)) |
| $K$ | 180 | – | Number of fiber orientations |
| $N$ | 11 | – | Number of generations |
| $K_g T_c/\rho_c$ | 5 | – | Ratio between the time constant of collagen degradation ($T_c$) and the time constant of collagen production ($\rho_c/K_g$) |
| $k$ | 1 | – | Scaling factor of the width of the fiber distribution (see (23)) |
| $\lambda_z$ | 1.3 | – | Axial physiological pre-stretch of the artery |
| $p_{ph}$ | 16 | kPa | Systolic blood pressure |
| Aneurysm (additional parameters) | | | |
| $T_m/T_c$ | 100 | – | Ratio between the time constants of matrix and collagen degradation, respectively |
| $k_m$ | 0.1 | – | Minimum fraction of the matrix left after the degradation stops |
| $L_d$ | 13 | mm | Axial half-length of the matrix degradation region |

Constitutive and loading parameters are given in Table 3. The values for the matrix shear modulus $c_m$ and material coefficients for collagen fibers $k_1$ and $k_2$ were calculated using material parameters for elastin, ground substance, and collagen from the media layer of the artery in Watton and Hill (2009). We note that the cumulative stiffness of collagen fibers according to (6) is equal to $n_{c,\mathrm{tot}}\, k_1$. The counterpart of this stiffness in Watton and Hill (2009) equals $n\, k_{\mathrm{M}}\, a_{\mathrm{x}}/4$, where $n$ is the collagen density relative to that in the healthy state, $k_{\mathrm{M}}$ is the material parameter for collagen in the media, and $a_{\mathrm{x}}$ is an exponential parameter for collagen. Taking into account that in the healthy state $n_{c,\mathrm{tot}} = n_{c,\mathrm{tot}}^H$ and $n = 1$, we get $k_1 = (k_{\mathrm{M}} a_{\mathrm{x}})/(4 n_{c,\mathrm{tot}}^H)$. Finally, on evaluating the latter relation using $k_{\mathrm{M}}$ and $a_{\mathrm{x}}$ from Watton and Hill (2009), and $n_{c,\mathrm{tot}}^H$ from Table 1 and rounding the result, we get the parameter $k_1$, given in Table 3. The homeostatic stretch $\lambda_c^{\mathrm{hom}}$ is equal to the attachment stretch in Watton and Hill (2009). A large value of $\kappa/c_m$ was used to enforce $J_g$ to be close to $J_g^{\mathrm{unc}}$. Discretization parameter $K$ was set to 180 to evaluate fiber density per degree. Via a numerical experiment, we determined that $N = 11$ generations was sufficient to ensure the independence of the numerical scheme of the time discretization: a reduction to $N = 9$ generations yielded a change in the loaded outer radius at homeostasis of only 0.5%. The ratio $K_g T_c/\rho_c$ was set to a value large enough to provide a stationary solution with the acceptable value of the averaged volume fraction of collagen. The scaling factor $k$ was taken from Driessen et al. (2008). Axial pre-stretch $\lambda_z$ of the artery

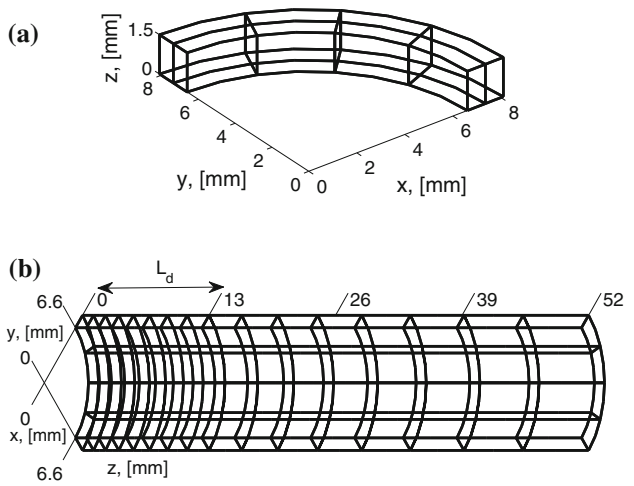


**Fig. 4** Unloaded mesh for finite element computations towards a healthy state (**a**), and for aneurysm computations (**b**). Due to circumferential symmetry of the problem and the presence of a symmetry plane $z = 0$, one eighth of the cylinder is used. Due to axial uniformity of the problem in **a** only one element in the axial direction is used

and blood pressure $p_{ph}$ were taken from Watton and Hill (2009).

The geometry of the artery is cylindrical. Both the problem of the healthy artery and the aneurysm are symmetric circumferentially and with respect to the $xy$-plane, allowing restriction of the computations to 1/8 part of the complete geometry. Since the healthy artery is uniform along the axial direction, we use only one element in this direction, see Fig. 4a. In case of the aneurysm, we use more elements in axial direction, to be able to capture axial variations, see Fig. 4b.

Boundary conditions during loading phase, complementing (9) are the following. The pressure $p_{ph}$ is applied at the inner surface, and the outer surface is kept free of stress. The displacements along the surfaces $x = 0$, $y = 0$ and $z = 0$, see Fig. 4 are suppressed in their normal directions, and an axial displacement corresponding to the axial stretch $\lambda_z$ (see Table 2) is applied to the surface $z = 1.5$.

Boundary conditions during growth phase, complementing (18) are the following. The inner surface of the artery is kept fixed, the outer surface is free of stress, and the displacements along $x = 0$, $y = 0$, $z = 0$ and $z = 1.5$ are suppressed in their normal directions.

In case of a healthy artery, no degradation of the matrix occurs. Therefore, the rate of the matrix degradation $\dot{m}_m(t)$ given by (15) equals to zero. In case of an aneurysm, the amount of the matrix per elementary reference (in the healthy state) volume decreases with time as the aneurysm grows. We define the volume fraction of the matrix with respect to the unloaded geometry in the healthy state $n_m^{\text{ref}}(t)$ as follows:

$$n_m^{\text{ref}}(t) = n_{m,H}\,[1 - (1 - q_m(t))S\,], \tag{32}$$

where $q_m(t)$ is a survival function of the matrix (which corresponds to transient matrix degradation), $S = S(\mathbf{x}_H)$ is a spatial degradation function of the matrix, $n_{m,H} = n_{m,H}(\mathbf{x}_H)$ is the volume fraction of the matrix with respect to the healthy state, and $\mathbf{x}_H$ is the position vector in the unloaded healthy configuration (see Fig. 4b). We assume a linear relation for the transient part:

$$q_m(t) = \begin{cases} 1 + \dfrac{t}{T_m}(k_m - 1), & 0 \le t \le T_m, \\ k_m, & t > T_m, \end{cases} \tag{33}$$

where $T_m$ is a characteristic time of the matrix degradation, and $k_m$ is the minimum fraction of the matrix left after the degradation stops. To preserve rotational symmetry, the spatial part of the degradation function depends on the axial coordinate $z$ only. We assume this function to be given by

$$S = S(z) = \begin{cases} 0.5\left(\cos\dfrac{\pi z}{L_d} + 1\right), & 0 \le z \le L_d, \\ 0, & z > L_d, \end{cases} \tag{34}$$

where $L_d$ is the half-length of the degradation region, see Fig. 4.

The values of the ratio $T_m/T_c$ and $k_m$ were taken from Watton et al. (2004), and the value of $L_d$ was tentatively chosen, see Table 3.

## 4 Results

### 4.1 Adaptation towards a healthy artery

The growth of the artery from the initial to the homeostatic state is characterized in Fig. 5. At the initial state, ($\hat{t} = t/T_c = 0$), the non-zero growth stimulus $\bar{\lambda}_c - \lambda_c^{\text{hom}}$, see Fig. 5a, triggers G&R of the tissue. As a result, the volume fraction of collagen increases as shown in Fig. 5b. Despite that, the radii of the loaded artery increase, indicating an increase of the tissue compliance, Fig. 5c. This increase in compliance is explained by the increase in the average recruitment stretch, Fig. 5d. The larger increase in the recruitment stretch at the inner surface of the artery than at the outer surface is explained by the larger tissue stretch at the inner surface than at the outer surface. As the growth stimulus diminishes, the volume fractions, the loaded radii, and the recruitment stretch asymptotically reach their stationary values at $\hat{t} = 3.5$. While the value of the time $\hat{t} = 3.5$ being 3.5 times the time constant of collagen half-life has no direct physiological relevance, it is important to note that the stationary healthy state is reached within a finite time.

The angular distribution of collagen fibers at the inner, the middle, and the outer surface of the artery at the homeostatic

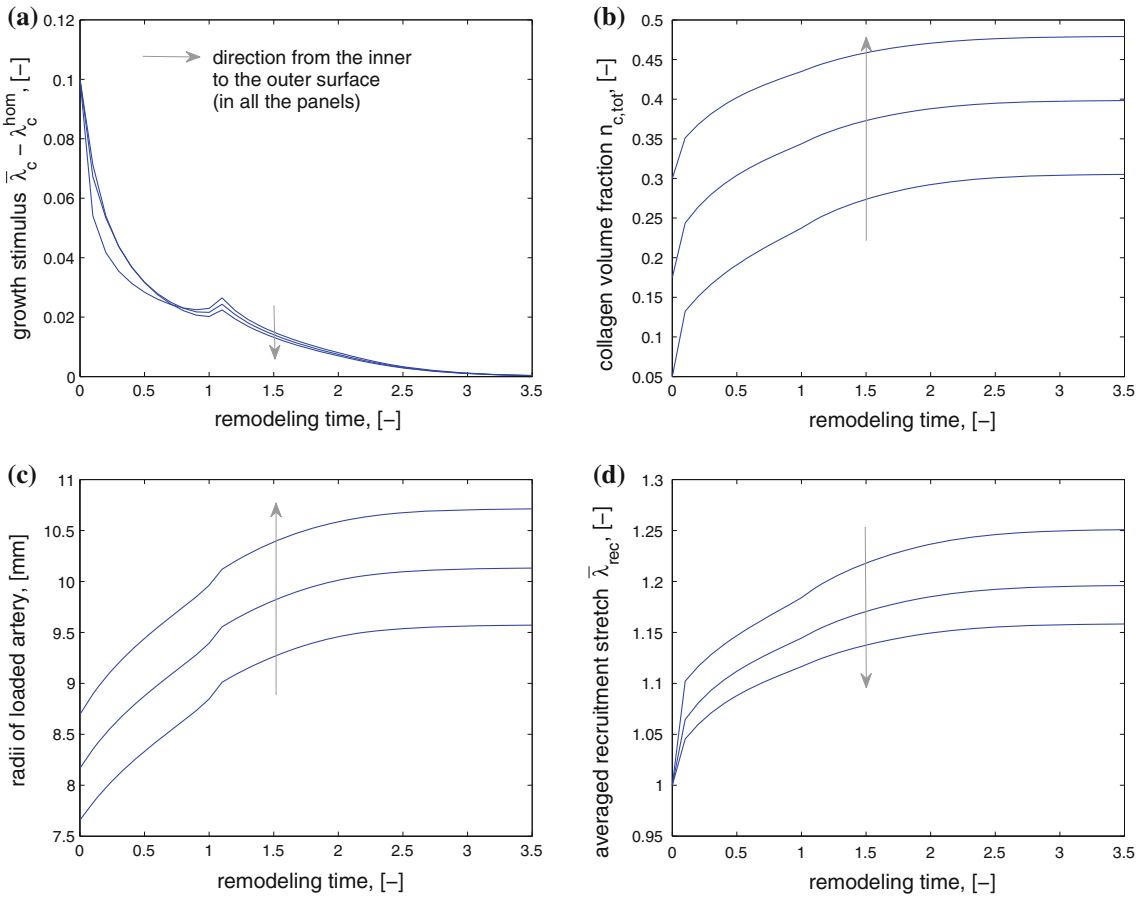


**Fig. 5** Time course of key quantities during development towards the healthy state, starting from the reference state at time 0. The time is scaled with respect to degradation time of collagen ($\hat{t} = t/T_c$). Non-zero growth stimulus (**a**) triggers an increase of collagen volume fraction (**b**). Despite an increase in collagen fraction, the artery becomes more compliant as displayed by an increase of the loaded radii (**c**). This is explained by the fact that new collagen is produced with a larger average recruitment stretch (**d**). The average recruitment stretch is defined in the same way as the average collagen stretch (11)

state is represented in Fig. 6 by the solid lines. At the inner surface of the artery, circumferential stretch is larger than axial stretch and fibers have a preference to the circumferential orientation. At the middle and the outer surface, circumferential and axial stretch are more similar and consequently, in line with (23) and (24), mean fiber direction is closer to 45 degrees, the width of the distribution is larger and the distribution is almost homogeneous.

#### *4.1.1 Parameter variation and sensitivity analysis*

The setting of several material and geometrical parameters is uncertain due to variation of these parameters with age, position along the aorta, and in between individuals. In addition, some model parameters cannot be measured directly. Therefore, it is important to study the behavior of the model in response to a variation of these parameters. It is also interesting to study the behavior of the model in response to a change in pressure load.

*Variation of growth rate*. Sensitivity of G&R to the setting of the ratio between time constants of collagen degradation and deposition, $K_g T_c/\rho_c$, was investigated through the response to a 25% increase in the blood pressure at homeostasis. The change of the outer radius of the artery with remodeling time is presented in Fig. 7a.

For $K_g T_c/\rho_c = 0$, no extra collagen is produced and the artery becomes weaker with time due to increased $\lambda_{rec}$ of new generations, which is reflected by a monotone unbounded increase in the loaded outer radius. By increasing the rate constant to $K_g T_c/\rho_c = 5$, the weakening of the tissue is counteracted by the strengthening caused by an increase in the collagen volume fraction and wall thickness (see Fig. 7b). Still, for this value of the rate constant, the radius of the artery keeps on increasing. Finally, for $K_g/\rho_c = 10$, the strengthening effect increases, and homeostasis is reached at $\hat{t} = 6$. With this, we conclude that the ratio $K_g T_c/\rho_c$ has a crucial effect on the stability of the solution at the homeostatic state. Time course of the wall thickness is presented in

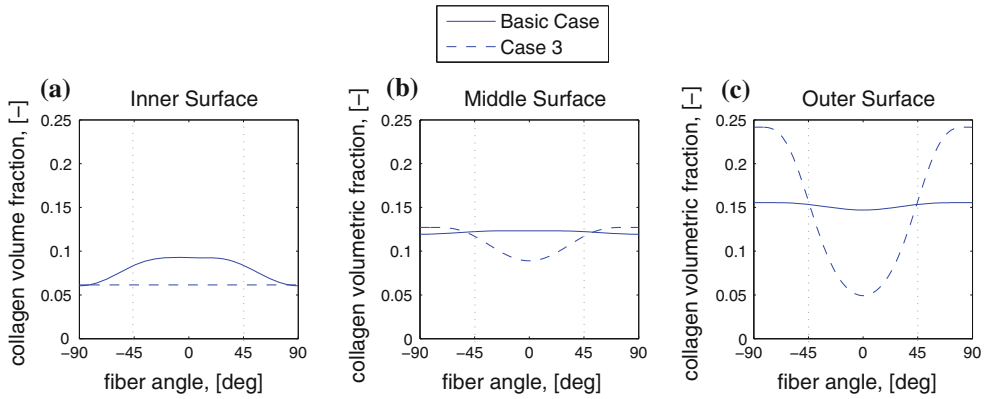


**Fig. 6** Distributions of collagen volume fractions ($\sum_{i=1}^{N} \hat{D}_i\, n_{c,i} = \hat{D}_1\, n_{\mathrm{c,tot}}$) at homeostatic state at the inner (**a**), the middle (**b**), and the outer (**c**) surface of the artery for the basic case (the *solid line*) and for the case 3 (the *dash line*), specified in Table 4. In the basic case, fiber orientations have a preference towards the circumferential orientation at the inner surface of the artery, no preferred direction at the middle surface, and a slight preference for the axial direction at the outer surface. In case 3, the fibers have no preferred direction at the inner surface, have preferred axial alignment at the middle surface, and even more preferred axial alignment at the outer surface

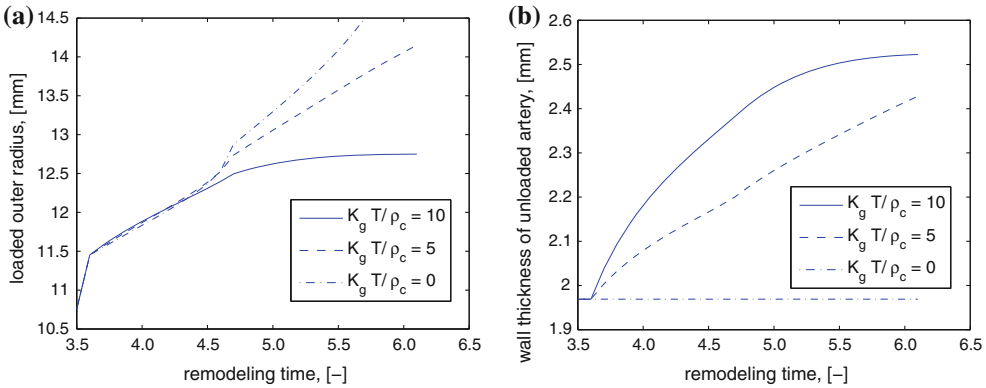


**Fig. 7** Outer radius versus dimensionless remodeling time after disturbing the homeostatic state with a 25% increase in pressure (**a**). An increase in pressure was applied at the first time-step, causing rapid increase of the radii. Depending on the ratio $K_g T_c/\rho_c$, the artery either reaches a new homeostatic state (for $K_g T_c/\rho_c = 10$), or keeps growing with time (for $K_g T_c/\rho_c = 0$ and $K_g T_c/\rho_c = 5$). The wall thickness of the artery (**b**) remains constant for $K_g T_c/\rho_c = 0$ since no extra collagen is produced. For $K_g T_c/\rho_c = 10$, the wall thickness reaches a stationary value (new homeostatic value), whereas for $K_g T_c/\rho_c = 5$ the wall thickness keeps on increasing, since no homeostatic state can be reached for this value

Fig. 7b. For $K_g T_c/\rho_c = 0$, the growth stimulus is zero resulting in no extra collagen production, and consequently no growth. As $K_g T_c/\rho_c$ increases, the wall thickness increases as well.

*Variation of the homeostatic stretch*. The other important parameter in the growth law (12) is the homeostatic collagen stretch $\lambda_c^{\mathrm{hom}}$. We investigated sensitivity to $\lambda_c^{\mathrm{hom}}$ by varying it in the reference state. The result is presented in Table 4 under case 1. Decreasing the homeostatic stretch of collagen makes the artery initially weaker leading to an increase in the outer radius and a decrease in the mean fiber directions. As compared to the basic case, at the inner surface the ratio of circumferential to axial stretch increases further above 1, leading to a more pronounced alignment of fibers in circumferential direction. At the outer surface, circumferential and axial stretch become more similar, mean fiber angle approaches 45 degrees and the width of the distribution increases. The growth stimulus at time $\hat{t} = 0$ (not shown in the table) increases as compared to the basic case, resulting in increased collagen volume fractions and the relative wall thickness.

*Variation of initial parameters*. The homeostatic state reached in our simulation also depends on the initial parameter settings, listed in Table 2. We consider two cases of variation of initial parameters, changing only one parameter value with respect to the basic state.

On increasing the initial recruitment of collagen fibers $\lambda_{\mathrm{rec}}^{(0)}$ (case 2 in Table 4), initially the tissue becomes weaker as compared with the basic case and consequently the loaded outer radius increases. However, $\bar{\lambda}_c$ decreases because of the increase in $\lambda_{\mathrm{rec}}^{(0)}$ and consequently the growth stimulus at the initial state decreases as well. Therefore, at homeostasis

**Table 4** Four cases of input parameter settings together with corresponding output parameters at homeostasis. The symbol '–' denotes the corresponding value in the basic case

| Parameter | Basic case | Case 1 | Case 2 | Case 3 |
|---|---|---|---|---|
| Input | | | | |
| Homeostatic collagen stretch $\lambda_c^{\text{hom}}$ [–] | 1.10 | 1.05 | – | – |
| Initial recruitment stretch $\lambda_{\text{rec}}^{(0)}$ [–] | 1.00 | – | 1.10 | – |
| Ratio of initial wall thickness to inner diameter $H^{(0)}/R_i^{(0)}$ [–] | 0.23 | – | – | 0.27 |
| Output | | | | |
| Wall thickness of unloaded artery, relative to the one in the reference state [–] | 1.31 | 1.38 | 1.24 | 1.22 |
| Outer radius of loaded artery [mm] | 10.75 | 11.08 | 11.83 | 9.99 |
| Collagen volume fraction averaged over the wall thickness [–] | 0.40 | 0.42 | 0.35 | 0.36 |
| $\mu_{\text{inner}}$ with respect to the circumferential direction [deg] | 33.2 | 30.8 | 24.8 | 44.9 |
| $\mu_{\text{outer}}$ with respect to the circumferential direction [deg] | 49.6 | 47.2 | 37.0 | 65.6 |
| $\sigma_{\text{inner}}$ [–] | 1.9 | 1.5 | 0.9 | 209.8 |
| $\sigma_{\text{outer}}$ [–] | 5.7 | 12.3 | 3.0 | 0.8 |

the relative wall thickness and the average collagen fraction are lower than in the basic case. As a result of the larger circumferential tissue stretch, mean fiber angles are closer to the circumference and this alignment is more pronounced, as is reflected by the decreased $\sigma_{\text{inner}}$ and $\sigma_{\text{outer}}$.

In case 3, the initial wall thickness is increased, making the artery stronger. As in case 2, the average collagen stretch decreases. This decrease yields a lower growth stimulus and consequently a decrease of the outer radius, the relative unloaded wall thickness, and the average collagen volume fraction at the homeostasis as compared with the basic case. At the inner surface, the reduced circumferential stretch is about equal to axial stretch, leading to a uniform distribution of fibers as shown by the dash lines in Fig. 6. At the outer surface, axial stretch dominates the reduced circumferential stretch more than in the basic case, and consequently a narrow distribution of fiber angles in axial direction is found.

### 4.2 Aneurysm growth

The healthy state is used as the reference state for aneurysm development, triggered by the degradation of the matrix described by (32). Figure 8 shows a numerical simulation of the shape of a developed fusiform aneurysm (a), illustrates the events at the location of largest matrix degradation (b–f), and displays the development of the aneurysm in an axial cross-section of the artery (g). The matrix degradation perturbs the equilibrium of the healthy state and thus induces increasing collagen stretches to attain a new mechanical equilibrium for the artery. This initiates a non-zero growth stimulus that increases as the degradation progresses over time, see Fig. 8b, and, according to (12), this yields an extra collagen production. Hence, similar to the case of G&R towards the healthy artery (Fig. 5), the collagen volume fraction increases, see Fig. 8c. The weakening effect associated with the matrix degradation and the increase in the recruitment stretch, see Fig. 8e, dominates the strengthening effect related to the increase of the collagen volume fraction. This can be seen from the monotone increase of the loaded radii throughout the complete period of matrix degradation in Fig. 8d. From the plot of the time course of the total volume change $J_g^{\text{tot}}$, shown in Fig. 8f, we notice that the volume decreases during the first half of the period of matrix degradation, but increases thereafter. This is because the volumetric effect of matrix degradation dominates over that of collagen production until about $t = 0.3T_m$, while the situation reverses thereafter. As soon as the degradation stops at $t = T_m$, the growth stimulus decays rapidly, and the aneurysm response reaches a steady state. The growth of the aneurysm shape at three time points during the degradation phase is displayed in Fig. 8g, where the deformed axial cross-section of the artery is shown.

## 5 Discussion

### 5.1 Results

The results of G&R towards a healthy artery demonstrate that our model converges to a stationary physiologically acceptable state of a healthy artery starting from a neighboring non-stationary state.

The results at the homeostatic state for the basic set of material parameters are consistent with data reported in literature, as explained below. The ratio $H/R_i$ of unloaded wall thickness to the unloaded radius at the homeostatic state equals 0.3, which is the same as the one in Watton and Hill (2009), and the circumferential stretch at 16 kPa blood

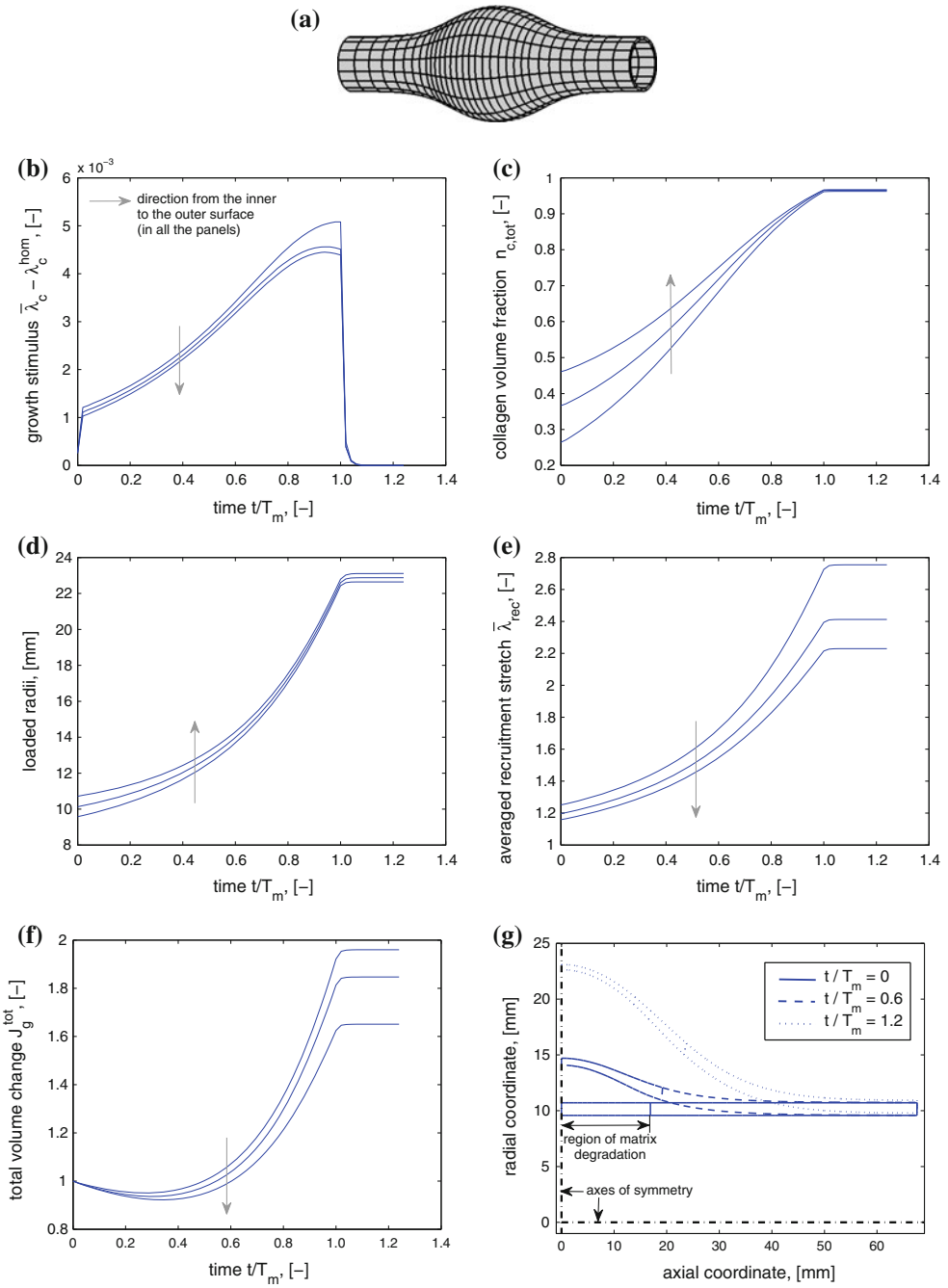


**Fig. 8** Simulation of aneurysm development; **a** simulated shape of a stabilized aneurysm; **b–f**: key quantities versus dimensionless time $t/T_m$ in the simulation of aneurysm development evaluated at $z = 0$ (the position of the largest diameter of the aneurysm). During the time interval $(0, T_m)$, the matrix degrades linearly in time; at $t = T_m$ degradation stops. Following the degradation, the growth stimulus increases (**b**), triggering a monotone increase of collagen volume fraction (**c**), loaded radii (**d**), and average recruitment stretch (**e**). Volumetric growth, represented by $J_g^{\text{tot}}$, **f** shows an initial decrease of volume followed by a later increase in volume. Growth of the aneurysm shape as displayed by the change of the axial cross-section of the loaded aneurysm (**g**)

pressure equals 1.44, which is close to 1.33 estimated from the mentioned study. The average collagen volume fraction $n_{c,\text{tot}} = 0.40$ (see the basic case in Table 4) is very close to the target value given in Table 1. In line with the observation by Fung (1993) that the collagen fraction is lower in the media than in the adventitia, and consistent with the abundance of collagen in the adventitia as reported by Rhodin (1980) and Wolinsky and Glagov (1964), we assumed a positive initial transmural gradient of the collagen fraction from inner to outer surface. This resulted in the found gradient of collagen

fraction in the healthy state (see Fig. 5b), which is in agreement with the literature observation mentioned above.

As concerns collagen fiber directions, experimentally it was found that fibers close to the inner surface are preferably aligned towards the circumferential direction, fibers near a middle surface have no preferential direction, and fibers close to the outer surface are mainly aligned towards the axial direction (Finlay et al. 1995; Wicker et al. 2008). Fiber distributions obtained with our model for the basic case of parameter setting display the same tendency, see Fig. 6 supported by numerical values in Table 4. Nevertheless, the mean fiber directions at the inner and the outer surfaces are less aligned with the circumferential and the axial direction, respectively, if compared with experimentally measured directions. We note that the mean fiber directions depend strongly on initial parameter settings (compare the dash and the solid lines in Fig. 6).

We studied the effect of variation of the dimensionless rate constant of collagen mass production under a 25% increase in the basal blood pressure. Alternatively, it might be considered as a prediction of the response to long-term hypertension. Stability of the solution depends on the rate of extra collagen production. For a stable solution, we observe an increase both in collagen volume fraction and in wall thickness of the artery (the lines corresponding to $K_g T_c/\rho_c = 10$, see Fig. 7*b*), which is in agreement with experimentally observed increase in collagen content and wall thickness reported by Hu et al. (2007). For too small values of $K_g T/\rho_c$, the homeostatic state becomes unstable. In this case, the strengthening due to an increase of collagen volume fraction is not sufficient to compensate for the weakening by increasing recruitment stretches of new collagen generations. It is interesting to note that, after adaptation to 20 kPa instead of 16 kPa, circumferential stress is increased by about 30% due to an increase in both the collagen and the matrix stress. The collagen stress increases due to higher collagen fraction and more circumferentially oriented fibers, and the matrix stress increases due to higher circumferential stretch.

G&R of the tissue is an interplay between stiffening associated with an increase of both collagen volume fraction and tissue volume and weakening related to deposition of new generations with a larger recruitment stretch. In case of G&R towards the healthy artery, the tissue being initially out of homeostatic equilibrium has a positive growth stimulus. In the first phase of the G&R-process, the weakening dominates over the strengthening thus increasing the compliance of the artery. However, as the growth stimulus decreases, the strengthening takes over from the weakening resulting in stabilizing the increase of compliance and reaching homeostasis as shown in Fig. 5.

In case of an aneurysm, triggered by matrix degradation, the growth stimulus increases during the whole period of matrix degradation and consequently tissue volume increases. Still, the associated strengthening effect is dominated by a weakening effect due to matrix degradation and increase of collagen recruitment stretch, and consequently aneurysm size keeps increasing (see Fig. 8). Only after the matrix degradation is complete, the growth stimulus decreases steeply, the strengthening takes over from weakening, and the aneurysm stabilizes. This leads to the shape of a developed stable fusiform aneurysm as shown in Fig. 8g. Stabilization of an aneurysm is supported by the observations that some aneurysms display no enlargement for years (Wermer et al. 2005).

## 5.2 Model

### *5.2.1 Volumetric growth and residual stress*

As outlined in the introduction, many models of arterial growth (e.g. Taber and Eggers 1996; Taber 1998; Rodriguez et al. 2007; Kuhl et al. 2007) are based on the model proposed by Skalak et al. (1982), Rodriguez et al. (1994). In these models, a growth stimulus is translated into a growth tensor, which describes the growth of infinitesimal tissue elements in a virtual, isolated state. To join the disconnected grown elements into a continuous structure, an additional elastic deformation is applied, giving rise to residual stress in the externally unloaded tissue. Experimentally, the presence of residual stress is reflected in the opening of arterial segments upon cutting them in longitudinal direction (see, e.g., Fung 1991).

The aforementioned growth studies consider the tissue as a one-component material, suggesting that the residual stress is borne by all tissue constituents. However, the latter conclusion is not in agreement with the observation by Greenwald et al. (1997), that elastin plays a key role in the opening angle of arteries, whereas the other two mechanically important tissue components, smooth muscle cells and collagen, have no effect on the opening angle. This suggests that residual stress is linked to elastin only. The observation by Greenwald et al. (1997) fits in elegantly with the constrained mixture approach, proposed by Humphrey and Rajagopal (2002). In this approach, tissue components are assumed to be in a state of continuous turnover and new components can be created at a stress-free state that differs from that of the old components. With respect to residual stress, the authors mention that "... in contrast to the concept of Skalak and others that residual stress results from locally incompatible growth in stress-free configurations, we suggest that residual stress relates more to differences between the deposition-stress and the stress in pre-existing material at the time of deposition, which is tantamount to saying differences in natural configurations." In addition, the observation that the turnover of elastin is negligibly slow in mature tissues (e.g., Langille 1996) as compared to that of the smooth muscle

cells and collagen suggests that elastin keeps its original reference state during the whole G&R process. In other words, the reference state for elastin (or natural state as called by Humphrey and Rajagopal) is the initial stress-free reference state and thus elastin is stretched in the unloaded (free of external loading) grown state, whereas collagen and smooth muscle cells are not. This implies that residual stress in the latter state is borne by elastin only, which is consistent with the observation by Greenwald et al. (1997) on the role of elastin as a carrier of residual stress.

In our model, we follow the constrained mixture approach and consider deposition and degradation of collagen generations, each with a unique stress-free state that is determined by the tissue loading at the time of creation. Moreover, following Humphrey and Rajagopal (2002) and Watton et al. (2004), collagen is undulated in the externally unloaded configuration, as expressed by the recruitment stretch $\lambda_{\text{rec}}$ that exceeds 1. Thus, unlike in models based on (Rodriguez et al. 1994), in our model collagen bears no (residual) stress in the externally unloaded state. Ideally, our model of growth should account for the constant stress-free state of elastin and the evolving stress-free states of smooth muscle cells as well. However, since we have lumped elastin and smooth muscle cells into one component, the matrix, we cannot distinguish between the contribution of smooth muscle cells and elastin to the stress. For now, we ignore the growth-induced stresses in the matrix, assuming that these stresses have faded at the end of the incremental growth. As a result, growth is described by evolving unloaded stress-free configurations. Obviously, our model might be improved by separating the contribution of smooth muscle cells and elastin allowing to keep track of the growth-induced stress in elastin, and enabling to obtain the residual stress in the unloaded configuration.

Our approach differs from that proposed by (Rodriguez et al. 1994) also in the actual description of growth. The growth tensor $\mathcal{F}_g^R$ used in these models describes incompatible growth of individual tissue elements. The subsequent elastic deformation gradient $\mathcal{F}_e^R$, needed to restore continuity of the tissue, is incompatible as well. The true, compatible, deformation gradient is the superposition of the two: $\mathcal{F}^R = \mathcal{F}_e^R \mathcal{F}_g^R$. So far, Rodriguez et al. (1994) and successors have defined the tensor $\mathcal{F}_g^R$ for specific (cylindrical) geometries only. Consequently, general 3D growth was not addressed. Our description of growth can be applied to arbitrary geometries. In our model, the growth is initiated locally by a scalar measure or growth stimulus $J_g^{\text{unc}}$. This stimulus is translated into the actually realized volume change $J_g$ by coupling the volumetric growth to the mechanical interaction between grown local tissue parts. We model this interaction by solving the mechanical interaction on the time scale of growth. The resulting compatible deformation gradient $\mathcal{F}_g$ (our counterpart of $\mathcal{F}^R$) already represents a combination of both growth and elastic deformation tensors, although these tensors are not specified separately.

The extent to which the unconstrained volume change resembles the real volume change depends on the ratio between $\kappa$ and $c_m$. At our setting of $\kappa/c_m = 100$, the difference between unconstrained and constrained growth was small: $\max |J_g^{\text{unc}}/J_g - 1| \approx 10^{-3}$.

### 5.2.2 Remodeling

In our model, we use the description of collagen architecture suggested by Driessen et al. (2008). In addition, we account for undulation of collagen fibers in the externally unloaded artery as in (Watton et al. 2004). Both studies make use of evolution equations for the description of collagen remodeling: two equations for the parameters of the distribution function for collagen orientation (Driessen et al. 2008, (10), (11)), and two equations for recruitment stretch and collagen density, respectively, (Watton et al. 2004, (32)). In our model, the evolution of the collagen distribution, recruitment stretch, and collagen volume fractions follow naturally with the evolution of collagen generations. The only evolution equation needed here is the equation for the rate of collagen production (12). In this way, we avoid introducing three extra evolution equations: one for the recruitment stretch, and two for the parameters of the collagen fiber distribution, thus reducing the number of assumptions and parameters.

### 5.2.3 Stimulus for G&R

As in many models of vascular growth, in our study, growth is initiated by a local mechanical stimulus. When the tissue is not in homeostasis, we assume an extra production of collagen given by the second term in the right-hand side of (12). This production is added to the production needed to compensate for the loss of collagen due to degradation (see (12)). This degradation is considered to be independent of mechanical tissue load, i.e., the survival function $q(t)$ in (28) is a function of time only. However, it has been demonstrated by Seliktar et al. (2003) and Lehoux et al. (2004) that matrix metalloproteinase (MMP) activity is upregulated following overstretching of the artery, resulting in accelerated collagen degradation. Our model could be extended in this respect by making the survival function a function of tissue stretch.

It is well known that, besides wall stress or strain, the shear rate imposed on the endothelial cells by the blood flow is an important trigger for vascular G&R (Dajnowiec and Langille 2007). The inner radius of an artery appears to adapt to changes of shear rate through both active contraction and growth of smooth muscle cells. In addition, vasoactive molecules regulated by the endothelium in response to altered wall shear stress affect extracellular matrix turnover (Malek and Izumo 1992; Uematsu et al. 1995). Our model does not

account in detail for these important parts of the artery's control mechanism. Instead, we assume our model artery to carry a constant flow, and approximate the result of adaptation to shear rate by fixing the inner radius during the growth simulation, accepting that the loaded inner radius still increases. Without this (crude) implementation of adaptation to shear rate, our simulations did not converge toward a stable homeostatic state. The studies by Alford et al. (2008) and Valentin et al. (2009) illustrate how the adaptation to shear rate could be modeled.

### 5.3 Conclusion

In conclusion, we presented a model of arterial G&R that combines the constrained mixture approach proposed by Humphrey and Rajagopal (2002) and the model for collagen architecture proposed by Driessen et al. (2008) with a novel concept of 3D tissue growth, induced by an extra production of collagen mass. The main limitations of the model are in lumping elastin and smooth muscle cells into one component, the matrix, and neglecting both residual stress and adaptation to shear rate.

We showed how the model could be used to arrive at a physiologically acceptable homeostatic state of the healthy artery. G&R following overpressure resulted in an increase of the wall thickness of the artery resembling similar observations *in vivo*. Stability of the artery upon changes in mechanical load was found to depend on the growth rate.

The model was also applied to the geometrically more complicated case of the development of a fusiform aneurysm triggered by a localized matrix degradation. Our simulation showed that aneurysm shape stabilized in time after the degradation was complete.



## References

Alford PW, Humphrey JD, Taber LA (2008) Growth and remodeling in a thick-walled artery model: effects of spatial variations in wall constituents. Biomech Model Mechanobiol 7(4):245–262

Baek SR, Rajagopal KR, Humphrey JD (2005) Competition between radial expansion and thickening in the enlargement of an intracranial saccular aneurysm. J Elast 80:13–31

Baek SR, Rajagopal KR, Humphrey JD (2006) A theoretical model of enlarging intracranial fusiform aneurysms. J Biomech Eng 128:142–149

Carmo M, Colombo L, Bruno A, Corsi F, Roncoroni L, Cuttin MS, Radice F, Mussini E, Settembrini PG (2002) Alteration of elastin, collagen and their cross-links in abdominal aortic aneurysms. Eur J Vasc Endovasc Surg 23(6):543–549

Dajnowiec D, Langille BL (2007) Arterial adaptations to chronic changes in haemodynamic function: coupling vasomotor tone to structural remodelling. Clin Sci (Lond) 113(1):15–23

Driessen NJB, Wilson W, Bouten CVC, Baaijens FPT (2004) A computational model for collagen fibre remodelling in the arterial wall. J Theor Biol 226:53–64

Driessen NJB, Bouten CVC, Baaijens FPT (2005) A structural constitutive model for collagenous cardiovascular tissues incorporating the angular fiber distribution. J Biomech Eng 127(3):494–503

Driessen NJB, Cox MAJ, Bouten CVC, Baaijens FPT (2008) Remodeling of the angular collagen fiber distribution in cardiovascular tissues. Biomech Model Mechanobiol 7(2):93–103

Feldman SA, Glagov S (1971) Transmedial collagen and elastin gradients in human aortas: reversal with age. Atherosclerosis 13(3):385–394

Finlay HM, McCullough L, Canham PB (1995) Three-dimensional collagen organization of human brain arteries at different transmural pressures. J Vasc Res 32(5):301–312

Frösen J, Piippo A, Paetau A, Kangasniemi M, Niemelä M, Hernesniemi J, Jääskeläinen J (2004) Remodeling of saccular cerebral artery aneurysm wall is associated with rupture: histological analysis of 24 unruptured and 42 ruptured cases. Stroke 35(10):2287–2293

Fung YD (1991) What are the residual stresses doing in our blood vessels? Ann Biomed Eng 19(3):237–249

Fung YC (1993) Biomechanics: mechanical properties of living tissues. Springer, New York

Gleason RL, Taber LA, Humphrey JD (2004) A 2-D model of flow-induced alterations in the geometry, structure, and properties of carotid arteries. J Biomech Eng 126(3):371–381

Greenwald SE, Moore JE, Rachev A, Kane TP, Meister JJ (1997) Experimental investigation of the distribution of residual strains in the artery wall. J Biomech Eng 119(4):438–444

Hariton I, deBotton G, Gasser TC, Holzapfel GA (2007) Stress-driven collagen fiber remodeling in arterial walls. Biomech Model Mechanobiol 6(3):163–175

He CM, Roach MR (1994) The composition and mechanical properties of abdominal aortic aneurysms. J Vasc Surg 20(1):6–13

Holzapfel GA, Gasser TC, Ogden RW (2000) A new constitutive framework for arterial wall mechanics and a comparative study of material models. J Elast 16:1–48

Hu JJ, Fossum TW, Miller MW, Xu H, Liu JC, Humphrey JD (2007) Biomechanics of the porcine basilar artery in hypertension. Ann Biomed Eng 35(1):19–29

Humphrey JD (1999) Remodeling of a collagenous tissue at fixed lengths. J Biomech Eng 121:591–597

Humphrey JD, Rajagopal KR (2002) A constrained mixture model for growth and remodeling of soft tissues. Math Model Method Appl Sci 12(3):407–430

Klisch SM, van Dyke TJ, Hoger A (2001) A theory of volumetric growth for compressible elastic biological materials. Math Mech Solids 6:551–575

Kroon M, Holzapfel GA (2007) A model for saccular cerebral aneurysm growth by collagen fibre remodelling. J Theor Biol 247(4):775–787

Kuhl E, Maas R, Himpel G, Menzel A (2007) Computational modeling of arterial wall growth. Biomech Model Mechanobiol 6:321–331

Langille BL (1996) Arterial remodeling: relation to hemodynamics. Can J Physiol Pharmacol 74:834–841

Lehoux S, Lemarie CA, Esposito B, Lijnen HR, Tedgui A (2004) Pressure-induced matrix metalloproteinase-9 contributes to early hypertensive remodeling. Circulation 109(8):1041–1047

Malek A, Izumo S (1992) Physiological fluid shear stress causes down-regulation of endothelin-1 mRNA in bovine aortic endothelium. Am J Physiol 263(2 Pt 1):C389–C396

Rachev A, Stergiopulos N, Meister JJ (1996) Theoretical study of dynamics of arterial wall remodeling in response to changes in blood pressure. J Biomech 29(5):635–642

Rhodin JAG (1980) Architecture of the vessel wall. In: Sparks HV Jr, Bohr DF, Somlyo AD, Geiger SR (eds) Handbook of physiology. The cardiovascular system, vol 2. American Physiological Society, Bethesda, pp 1–31

Rodriguez EK, Hoger A, McCulloch AD (1994) Stress-dependent finite growth in soft elastic tissues. J Biomech 27(4):455–467

Rodriguez J, Goicolea JM, Gabaldon F (2007) A volumetric model for growth of arterial walls with arbitrary geometry and loads. J Biomech 40(5):961–971

Segal A (2007) SEPRAN programmers guide, standard problems, users manual, manual examples, manual user examples, theoretical manual. Ingenieursbureau SEPRA, Den Haag

Seliktar D, Nerem RM, Galis ZS (2003) Mechanical strain-stimulated remodeling of tissue-engineered blood vessel constructs. Tissue Eng 9(4):657–666

Skalak R, Dasgupta G, Moss M, Otten E, Dullumeijer P, Vilmann H (1982) Analytical description of growth. J Theor Biol 94(3):555–577

Taber LA (1998) A model for aortic growth based on fluid shear and fiber stresses. J Biomech Eng 120:348–354

Taber LA (2000) Pattern formation in a nonlinear membrane model for epithelial morphogenesis. Acta Biotheor 48:47–63

Taber LA, Eggers DW (1996) Theoretical study of stress-modulated growth in the aorta. J Theor Biol 180(4):343–357

Taber LA, Humphrey JD (2001) Stress-modulated growth, residual stress, and vascular heterogeneity. J Biomech Eng 123(6):528–535

Uematsu M, Ohara Y, Navas JP, Nishida K, Murphy TJ, Alexander RW, Nerem RM, Harrison DG (1995) Regulation of endothelial cell nitric oxide synthase mRNA expression by shear stress. Am J Physiol 269(6 Pt 1):C1371–C1378

Valentin A, Cardamone L, Baek S, Humphrey JD (2009) Complementary vasoactivity and matrix remodelling in arterial adaptations to altered flow and pressure. J R Soc Interface 6(32):293–306

Watton PN, Hill NA (2009) Evolving mechanical properties of a model of abdominal aortic aneurysm. Biomech Model Mechanobiol 8(1):25–42

Watton PN, Hill NA, Heil M (2004) A mathematical model for the growth of the abdominal aortic aneurysm. Biomech Model Mechanobiol 3:98–113

Watton PN, Ventikos Y, Holzapfel GA (2009) Modelling the growth and stabilization of cerebral aneurysms. Math Med Biol 26(2):133–164

Wermer MJ, van der Schaaf IC, Velthuis BK, Algra A, Buskens E, Rinkel GJ (2005) Follow-up screening after subarachnoid haemorrhage: frequency and determinants of new aneurysms and enlargement of existing aneurysms. Brain 128:2421–2429

Wicker BK, Hutchens HP, Wu Q, Yeh AT, Humphrey JD (2008) Normal basilar artery structure and biaxial mechanical behaviour. Comput Methods Biomech Biomed Eng 11(5):539–551

Wolinsky H, Glagov S (1964) Structural basis for the static mechanical properties of the aortic media. Circ Res 14:400–413